# Recent results for the one-proton transfer reaction in the $^{18}$O+$^{48}$Ti collision at 275 MeV

*O.* Sgouros[1,*], *M.* Cavallaro[1], *F.* Cappuzzello[1,2], *D.* Carbone[1], *C.* Agodi[1], *C.* Altana[1], *G. A.* Brischetto[1,2], *S.* Burrello[3,4], *S.* Calabrese[1], *D.* Calvo[5], *V.* Capirossi[5,6], *E. R.* Chávez Lomelí[7], *I.* Ciraldo[1,2], *M.* Cutuli[1,2], *G.* De Gregorio[8,9], *F.* Delaunay[1,2,10], *H.* Djapo[11], *C.* Eke[12], *P.* Finocchiaro[1], *M.* Fisichella[1], *A.* Foti[13], *A.* Gargano[8], *A.* Hacisalihoglu[14], *F.* Iazzi[5,6], *L.* La Fauci[1,2], *R.* Linares[15], *J.* Lubian[15], *N. H.* Medina[16], *M.* Moralles[17], *J. R. B.* Oliveira[15], *A.* Pakou[18], *L.* Pandola[1], *F.* Pinna[5,6], *G.* Russo[2,13], *M. A.* Guazzelli[19], *V.* Soukeras[1], *G.* Souliotis[20], *A.* Spatafora[1,2], *D.* Torresi[1], *A.* Yildirim[21], and *V. A. B.* Zagatto[15] for the NUMEN collaboration

[1]INFN - Laboratori Nazionali del Sud, Catania, Italy
[2]Dipartimento di Fisica e Astronomia "Ettore Majorana", Università di Catania, Catania, Italy
[3]Université Paris-Saclay, CNRS/IN2P3, IJCLab, Orsay, France
[4]Technische Universität Darmstadt, Institut für Kernphysik, Darmstadt, Germany
[5]INFN - Sezione di Torino, Torino, Italy
[6]DISAT - Politecnico di Torino, Torino, Italy
[7]Instituto de Física, Universidad Nacional Autónoma de México, Mexico City, Mexico
[8]INFN - Sezione di Napoli, Napoli, Italy
[9]Dipartimento di Matematica e Fisica, Università della Campania "Luigi Vanvitelli", Caserta, Italy
[10]LPC Caen, Normandie Université, ENSICAEN, UNICAEN, CNRS/IN2P3, Caen, France
[11]Ankara University, Institute of Accelerator Technologies, Turkey
[12]Department of Mathematics and Science Education, Faculty of Education, Akdeniz University, Antalya, Turkey
[13]INFN - Sezione di Catania, Catania, Italy
[14]Institute of Natural Sciences, Karadeniz Teknik Universitesi, Trabzon, Turkey
[15]Instituto de Física, Universidade Federal Fluminense, Niterói, Brazil
[16]Instituto de Física, Universidade de São Paulo, São Paulo, Brazil
[17]Instituto de Pesquisas Energeticas e Nucleares IPEN/CNEN, São Paulo, Brazil
[18]Department of Physics, University of Ioannina and Hellenic Institute of Nuclear Physics, Ioannina, Greece
[19]Centro Universitario FEI, São Bernardo do Campo, Brazil
[20]Department of Chemistry, University of Athens and Hellenic Institute of Nuclear Physics, Athens, Greece
[21]Department of Physics, Akdeniz Universitesi, Antalya, Turkey

**Abstract.** The $^{18}$O+$^{48}$Ti reaction was studied at the energy of 275 MeV for the first time under the NUMEN and NURE experimental campaigns with the aim to investigate the complete net of reaction channels potentially involved in the $^{48}$Ca→$^{48}$Ti double charge exchange transition. Such a transition is of great interest because of its relevance to the extraction of $^{48}$Ca→$^{48}$Ti double beta decay nuclear matrix element. The relevant experiment was carried out at the MAGNEX facility of INFN-LNS in Catania. Angular distribution measurements for the various reaction products were performed by using the MAGNEX large acceptance magnetic spectrometer. The present contribution is focused on the analysis of the one-proton transfer channel with emphasis on the particle identification technique and the estimation of background contaminations.

## 1 Introduction

The interest of the Nuclear Physics community for the Double Charge Exchange (DCE) reactions is still vivid due to their possible relation with the double beta ($\beta\beta$) decay [1]. Into this context, a novel idea has been recently conceived at Istituto Nazionale di Fisica Nucleare – Laboratori Nazionali del Sud (INFN-LNS), under the NUMEN (NUclear Matrix Elements for Neutrinoless double beta decay) project [2]. This is to use for the first time DCE reactions induced by heavy-ion beams as a mean for the determination of the $\beta\beta$ decay Nuclear Matrix Elements (NMEs). This unique opportunity is based on the fact that the two processes present some interesting similarities. Among them, both processes probe the same initial and final nuclear wave functions and the operators connecting them have a similar spin – isospin mathematical structure [2–4]. Thus, even if the two processes are mediated by different interactions, the involved NMEs could be connected and the determination of the DCE reaction cross-sections may provide an important piece of information on the $\beta\beta$ matrix elements. In the present study, which is a part of the

*e-mail: onoufrios.sgouros@lns.infn.it

NURE project [5], the $^{18}$O+$^{48}$Ti reaction was investigated by measuring not only the DCE channel, but also Single Charge Exchange (SCE) and multi-step transfer reactions which may lead to the same final states as the DCE one. It is very important to quantify possible contributions from other reaction channels to the DCE one for a precise determination of the absolute DCE cross sections, which may be the key for accessing the information of the NMEs of the $\beta\beta$ decay. In the present contribution, the data analysis of the one-proton transfer reaction $^{48}$Ti($^{18}$O,$^{19}$F)$^{47}$Sc is presented. The experimental details are presented in Section 2, while the data reduction procedure is reported in Section 3. Our results are summarized in Section 4.

## 2 Experimental Setup

The experiment was performed at the MAGNEX facility [6] of INFN-LNS, where an $^{18}O^{8+}$ beam accelerated by the K800 Superconducting Cyclotron at the energy of 275 MeV impinged onto a $TiO_2$ target 510 $\mu$g/cm$^2$ thick. An aluminum foil with a thickness of 216 $\mu$g/cm$^2$ was used as a backing for the target material. In order to estimate the background originating from the different target components, two additional runs, one with a pure $^{27}$Al target 226 $\mu$g/cm$^2$ thick and a $WO_3$ one (284 $\mu$g/cm$^2$) evaporated on a thin aluminium foil, were also performed. The various reaction products were momentum analyzed by the MAGNEX large acceptance magnetic spectrometer whose optical axis was set at $\theta_{opt}$= 9° with respect to the beam direction, spanning an angular range between 4° and 15° in the laboratory reference frame. The vertical slits of the MAGNEX spectrometer, located 260 mm downstream the target position were set such as to cover a vertical angular range of ±2°. The various reaction products emerging from the beam-target interaction were detected by the MAGNEX Focal Plane Detector (FPD) [7, 8].

The MAGNEX FPD is consisted of a gas section followed by a wall of 60 single silicon detectors. The use of the gas detector is twofold. It serves as a proportional drift chamber providing the energy loss signal ($\Delta$E) of the ions inside the gas, but also as a mean to map the ions track. The tracker is divided in six sections each one having at the top a proportional wire (DC) in which the ($\Delta$E) signal is measured. The sum of the 6 signals, $\Delta E_{tot}$, is used in the particle identification process. Above the DC wires, a set of 6 segmented anode strips is located where each strip is composed of 224 induction pads allowing the measurement of the horizontal position ($X_{foc}$) and thus, the determination of the horizontal angle ($\theta_{foc}$). Moreover, the electron drift time measurements inside the gas allow the determination of the vertical position ($Y_{foc}$) and angle ($\phi_{foc}$). With the present gas tracker, the maximum rate that the detector can sustain is limited to a few kHz. However, this will be insufficient for the future NUMEN experiments at the MAGNEX facility with high intensity beams. To this extent, the development of a new configuration [9, 10] for the MAGNEX FPD is in progress based on the THick GEM (THGEM) technology for the new tracker.

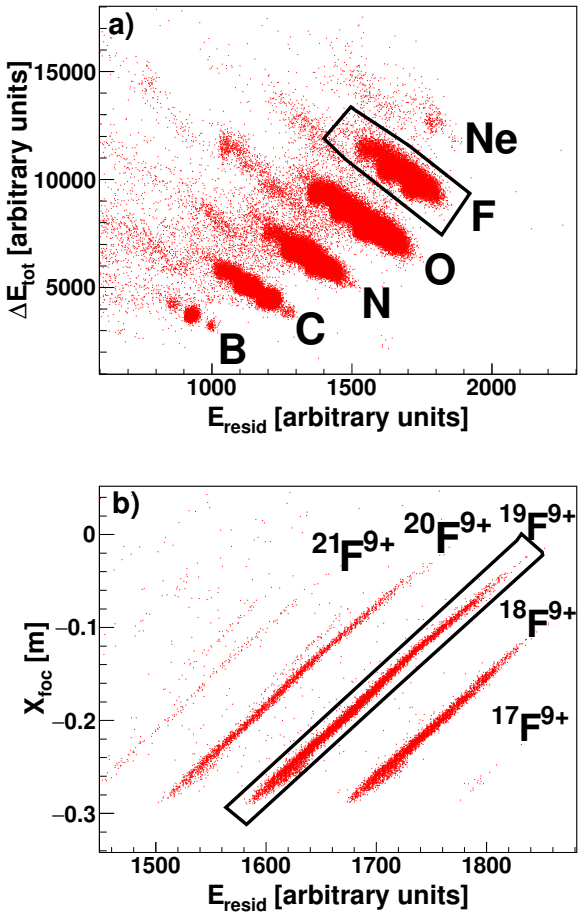


**Figure 1.** Typical particle identification spectra for the $^{48}$Ti($^{18}$O,$^{19}$F)$^{47}$Sc reaction at the energy of 275 MeV. a) $\Delta E_{tot}$ as a function the of residual energy, $E_{resid}$, measured by one silicon detector of the FPD. A graphical selection of the fluorine ion events is illustrated by the solid black line. b) The horizontal position at the MAGNEX focal plane, $X_{foc}$, as a function of the residual energy gated by the selected fluorine ions of panel (a). The different loci correspond to ions with different $\sqrt{m}$/q. A graphical selection on the $^{19}F^{9+}$ events is shown by the solid black line.

## 3 Data Reduction

The data analysis relies on the accurate identification of the reaction channel of our interest. The particle identification (PID) is the first step of the data analysis which was performed following the prescription of Ref. [11]. The various ion species were well-discriminated using the conventional $\Delta$E–E technique. A typical $\Delta E_{tot}$–$E_{resid}$ spectrum is presented in the top panel of Figure 1 for a single silicon detector. It is evident that the fluorine isotopes, highlighted with the black contour, are well separated from any other ion family. However, we are interested in identifying the one-proton pick up reaction products i.e. $^{19}F^{9+}$ so, the Z separation is not enough. To this direction, after the identification of the fluorine ions, the mass separation is feasible via the $X_{foc}$–$E_{resid}$ (horizontal position versus

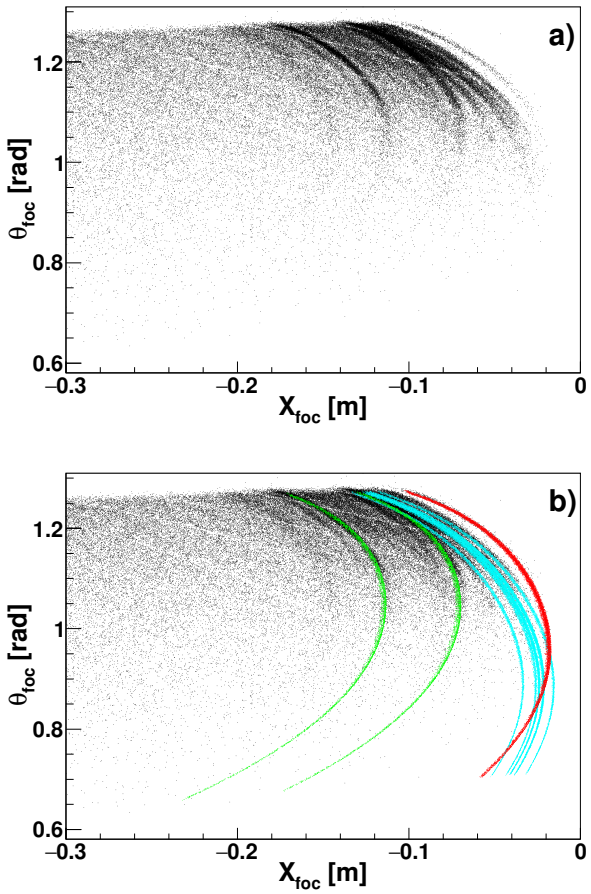


**Figure 2.** a) Correlation plot between the horizontal angle, $\theta_{foc}$, and horizontal position, $X_{foc}$, measured by the focal plane detector of the MAGNEX spectrometer. b) A comparison between the experimental data of panel (a) with the simulated ones for three different reaction channels. The red, cyan and green points correspond to the simulated events originating from the one-proton transfer reaction on $^{27}$Al, $^{48}$Ti and $^{16}$O target, respectively. For reasons of clarity, the simulations were performed only for a few selective transitions for the one-proton transfer reaction on each target.

residual energy measured for each silicon detector) spectra. In a spectrometer, the position along the dispersive axis is analogous to the momentum of the ion. So, the position and the energy are related according to the following expression:

$$X_{foc} \propto \frac{\sqrt{m}}{q} \sqrt{E_{resid}}, \quad (1)$$

where m, q and $E_{resid}$ are the ions' mass, charge state and residual energy, respectively. Ions possessing a different mass over charge state ratio lie on a different region at the $X_{foc}$–$E_{resid}$ representation as it is illustrated in the lower panel of Figure 1. Looking at Figure 1 it is obvious that the mass resolution of MAGNEX is excellent. Thus, the ΔE–E technique in conjunction with mass separation method presented above, provide the root for an accurate identification of the one proton pick-up reaction channel.

Once the $^{19}F^{9+}$ ions were identified, we have proceeded with the analysis of the the final phase space parameters. A typical $\theta_{foc}$-$X_{foc}$ spectrum obtained with the $TiO_2$+$^{27}$Al target is presented in Figure 2, where various loci are well-pronounced in the spectrum. Since a compound target was used in the current measurement, background events due to the reaction of the $^{18}$O beam with the oxygen and aluminium components of the target were also present in our spectra. In order to identify the fingerprint of each reaction, dedicated Monte Carlo simulations by taking into account the reaction kinematics but also the complete geometry of the spectrometer and the spatial distribution of the dipole and quadrupole fields were performed. The results of the simulations are compared to the experimental data in the lower panel of Figure 2. It is seen that the simulations describe in an excellent way the experimental data giving further support to the validity of the dipole and quadrupole fields which were adopted in the simulations. The different slope met both in experimental and simulated events is attributed partially to the different kinematics for each reaction and partially to the chromatic aberrations which are present in large-acceptance optical devices like MAGNEX. However, the latter are effectively compensated when a high-order software trajectory reconstruction [12] is applied to the data.

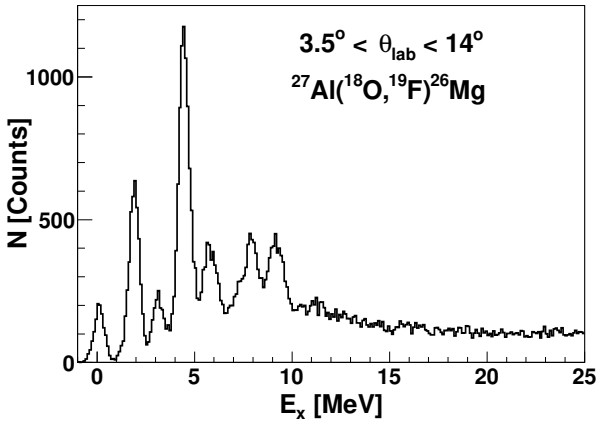


**Figure 3.** Reconstructed excitation energy spectrum for the $^{27}$Al($^{18}$O,$^{19}$F)$^{26}$Mg reaction at 275 MeV.

Having identified the background events, the analysis of the data obtained with the pure aluminum target and the $WO_3$+$^{27}$Al one was performed in order to estimate and subtract the contaminant events in the data set obtained with the $TiO_2$+$^{27}$Al target. A software ray reconstruction was applied to the data and the initial phase space parameters (e.g. $\theta_{lab}$, kinetic energy) were reconstructed from the measured ones (e.g. $\theta_{foc}$, $\phi_{foc}$, $X_{foc}$). The excitation energy $E_x$ was determined from the missing mass method [6] as:

$$E_x = Q_0 - Q, \quad (2)$$

where $Q_0$ is the ground state (g.s.) to g.s. transition. The reconstructed excitation energy spectrum for the data obtained with aluminum target is presented in Figure 3.

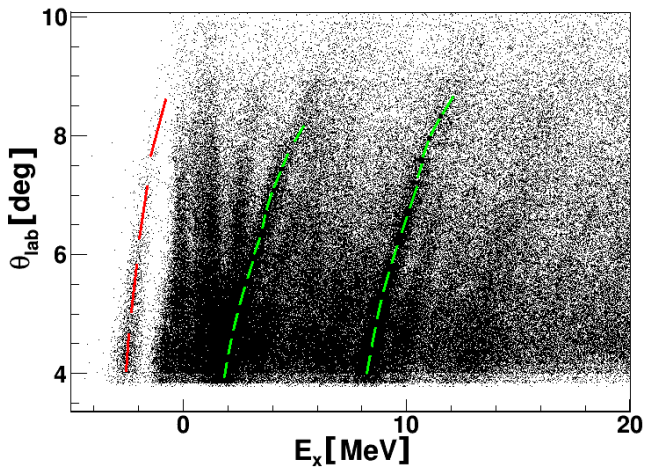


**Figure 4.** Bi-dimensional plot for the reconstructed scattering angle, $\theta_{lab}$, as a function of the excitation energy, $E_x$, for the data obtained with the $TiO_2$+$^{27}$Al target. The inclined loci, highlighted with the dashed-green and long-dashed red curves, correspond to the one-proton transfer reaction of $^{18}$O with the oxygen and aluminum components of the target, respectively. The vertical loci correspond to the reconstructed events from the reaction on the $^{48}$Ti target.

Various peaks associated to transition to the states of $^{19}$F and $^{26}$Mg nuclei are well-formed in the spectrum up to the excitation energy of 10 MeV, where a rather continuum shape is observed due to the decay of $^{26}$Mg nucleus ($^{26}$Mg→$^{22}$Ne+$\alpha$). A similar procedure was also followed for the data obtained with the $WO_3$+$^{27}$Al target and the excitation energy spectrum corresponding to the $^{16}$O($^{18}$O,$^{19}$F)$^{15}$N reaction was deduced. After completing the analysis of the background runs, the same trajectory reconstruction technique was applied to the data obtained with the $TiO_2$+$^{27}$Al target. The reconstructed $\theta_{lab}$-$E_x$ plot is shown in Figure 4. Like in case of Figure 2, we can immediately identify in the spectrum the presence of the reaction contaminants. For reasons of clarity, we have pointed-out a few selected transitions. The inclined locus, highlighted with the red long-dashed curve, correspond to the g.s. of the $^{27}$Al($^{18}$O,$^{19}$F)$^{26}$Mg reaction, while the ones illustrated with the green dashed curves correspond to the g.s. and the 6.324 MeV ($3/2^-$) state of $^{15}$N from the $^{16}$O($^{18}$O,$^{19}$F)$^{15}$N reaction. The vertical oriented loci correspond to the $^{19}$F and $^{47}$Sc states populated in the $^{48}$Ti($^{18}$O,$^{19}$F)$^{47}$Sc reaction. In order to isolate the energy spectrum for the one-proton transfer reaction on $^{48}$Ti, after projecting the data of Figure 4 onto the $E_x$ axis, we have superimposed to the mixed spectrum the previously analyzed data with the aluminum and oxygen targets, appropriately normalized. Subsequently, the background spectra were subtracted from the mixed one and the energy spectrum corresponding to the $^{48}$Ti($^{18}$O,$^{19}$F)$^{47}$Sc reaction was deduced. The background subtraction procedure is presented in Figure 5. As it can be seen, the energy spectrum corresponding to the $^{48}$Ti($^{18}$O,$^{19}$F)$^{47}$Sc reaction is rather structure-less as a result of the high density of states of the $^{47}$Sc nucleus. The data analysis for the reaction under study was recently completed and the results have been submitted for publication.

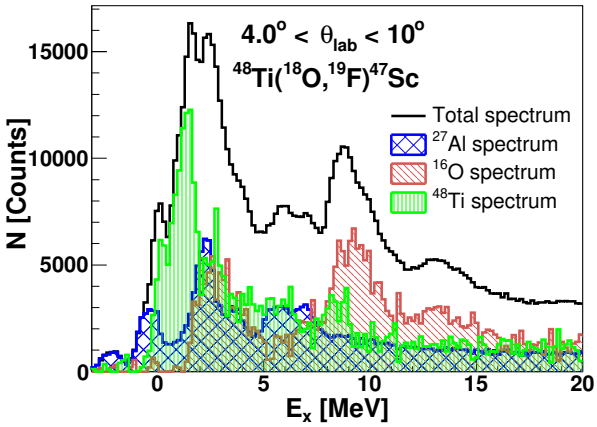


**Figure 5.** Decomposition of the excitation energy spectrum obtained with the $TiO_2$+$^{27}$Al target. The total spectrum is presented with the solid black line. The blue-hatched area corresponds to the normalized background originating from the $^{27}$Al backing material, while the brown solid line corresponds to the background arising from oxygen. The green solid line is the obtained excitation energy spectrum for the $^{48}$Ti($^{18}$O,$^{19}$F)$^{47}$Sc reaction, after subtracting from the total spectrum the background contributions.

## 4 Summary

The study of the $^{18}$O+$^{48}$Ti reaction at 275 MeV was performed, for the first time, at INFN-LNS under the NUMEN and NURE experimental campaigns. Angular distribution measurements for the $^{48}$Ti($^{18}$O,$^{19}$F)$^{47}$Sc reaction were performed by using the MAGNEX large acceptance magnetic spectrometer. Complementary measurements with aluminum and $WO_3$+$^{27}$Al targets of the appropriate thickness were performed in order to estimate the background arising from the use of a $TiO_2$ target evaporated onto a thin aluminum foil. After subtracting the background contamination, the excitation energy spectrum corresponding to the $^{48}$Ti($^{18}$O,$^{19}$F)$^{47}$Sc reaction was deduced. Given the high density of states of the populated $^{47}$Sc nucleus and the finite experimental energy resolution (about 500 keV FWHM) the measured excitation energy spectrum was rather structure-less. The results of this analysis will be the subject of a forthcoming publication.

## Acknowledgments

The research leading to these results was partially funded by the European Research Council (ERC) under the European Union's Horizon 2020 Research and Innovation Programme (Grant Agreement No 714625).

## References

[1] H. Ejiri, J. Suhonen and K. Zuber, Phys. Rep. **797**, 1 (2019)

[2] F. Cappuzzello, C. Agodi, M. Cavallaro et al., Eur. Phys. J. A **54**, 72 (2018)

[3] E. Santopinto, H. García-Tecocoatzi, R. I. Magaña Vsevolodovna et al., Phys. Rev. C **98**, 061601(R) (2018)

[4] H. Lenske, F. Cappuzzello, M. Cavallaro et al., Prog. Part. Nucl. Phys. **109**, 103716 (2019)

[5] M. Cavallaro, E. Aciksoz, L. Acosta et al., POS **302**, (BORMIO2017) 015 (2017)

[6] F. Cappuzzello, C. Agodi, D. Carbone et al., Eur. Phys. J. A **52**, 167 (2016)

[7] M. Cavallaro, F. Cappuzzello, D. Carbone et al., Eur. Phys. J. A **48**, 59 (2012)

[8] D. Torresi, O. Sgouros, V. Soukeras et al., Nucl. Instrum. Methods Phys. Res. A **989**, 164918 (2021)

[9] C. Agodi, A. D. Russo, L. Calabretta et al., Universe **7**, 72 (2021)

[10] F. Cappuzzello, L. Acosta, C. Agodi et al., Front. Astron. Space. Sci. **8**, 668587 (2021)

[11] F. Cappuzzello, M. Cavallaro, A. Cunsolo et al., Nucl. Instrum. Meth. A **621**, 419 (2010)

[12] F. Cappuzzello, D. Carbone, M. Cavallaro, Nucl. Instrum. Methods Phys. Res. A **638**, 74 (2011)

[13] M. Cavallaro, F.Cappuzzello, D.Carbone et al., Nucl. Instrum. Meth. A **637**, 77 (2011)